ACS APPLIED MATERIALS & INTERFACES

Research Article

www.acsami.org

Blue-Emitting Copper Nanoclusters Synthesized in the Presence of Lysozyme as Candidates for Cell Labeling

Rama Ghosh,[†] Amaresh Kumar Sahoo,[‡] Siddhartha Sankar Ghosh,[‡,§] Anumita Paul,*[,†] and Arun Chattopadhyay*[,†,‡]

[†]Department of Chemistry, [‡]Centre for Nanotechnology, and [§]Department of Biotechnology, Indian Institute of Technology Guwahati, Guwahati-781039, India

Supporting Information

ABSTRACT: Highly fluorescent copper nanoclusters (Cu NCs) have been synthesized using single-step reduction of copper sulfate by hydrazine in the presence of lysozyme. The fluorescence quantum yield was measured to be as high as 18%. The emission was also found to be dependent on the excitation wavelength. Mass spectrometric analyses indicated the presence of species corresponding to Cu_2 to Cu_9. Transmission electron microscopic analyses indicated the formation of agglomerated particles of average diameter of 2.3 nm, which were constituted of smaller particles of average diameter of 0.96 nm. They were found to be stable between pH 4 and 10 and in addition having excellent chemical and photostability. The noncytotoxic NCs were used to successfully label cervical cancer HeLa cells.

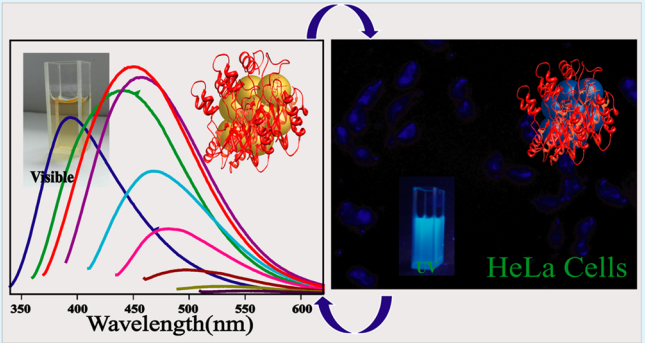

KEYWORDS: *copper nanoclusters, fluorescence, HeLa cells, photostability, cytotoxicity*

INTRODUCTION

Stabilizing nanoclusters (NCs) of noble metal remains the primary challenge in their syntheses and applications. It has been proposed that these highly luminescent and photostable NCs could substitute toxic quantum dots in bioimaging and biolabeling.[1,2] In this regard, owing to their redox properties, NCs of gold (Au), and to some extent those of silver (Ag), have been stabilized with considerable success in comparison to those of copper (Cu). For example, recently, syntheses of luminescent Au and Ag NCs have been reported using dendrimers,[3] poly(acrylic acid) polymer,[4,5] DNA,[6,7] and protein[8] as stabilizers. Among the proteins, bovine serum albumin,[8−10] lacto transferrin,[11] lysozyme,[12,13] insulin,[14] horseradish peroxidase,[15] and pepsin[16] have been preferred as stabilizers. It is important to mention here that the proposed use of these clusters in a biological environment demands their stability in an aqueous medium. This has remained a challenge for the synthesis of NCs of Cu. The ease of oxidation of Cu (E^0, 0.34 V), in comparison to that of Ag (E^0, 0.80 V) and Au (E^0, 1.50 V), has limited progress in the development of synthetic methods, especially in an aqueous medium. A recent report indicates that Cu NCs of less than 3 nm, synthesized using a polyol method under a N_2 atmosphere, were stable following their redispersion in an aqueous medium.[17] On the other hand, the possibility of the synthesis of small Cu NCs in an aqueous medium electrochemically has also been demonstrated.[18] Interestingly, DNA-hosted Cu NCs, synthesized in the presence of ascorbic acid, have been used for the identification of single nucleotide polymorphism.[19] However, there is a need for the development of aqueous-based synthetic methods for versatile use, especially in biological applications. Cu is an important trace element, being present in the human body as an essential catalytic cofactor in redox-active enzymes such as cytochrome *c* oxidase and lysyl oxidase. The permissible intake of Cu for an adult is 0.6−1.6 mg/day.[20] The ease of sequestration of Cu by a natural bodily mechanism and the availability of commercial chelating agents also make its use relatively friendly in human subjects over those of Au and Ag, especially at low concentrations.[21,22]

Herein we report the synthesis of highly fluorescent, blue-emitting Cu NCs by chemical reduction of $CuSO_4$ in an aqueous medium, in the presence of lysozyme. Lysozyme, a 14.3 kDa protein, has 129 amino acid residues including 8 cysteine residues. The antimicrobial protein is biocompatible and has been a favorite as a stabilizer of Au NCs.[13] The so-synthesized protein-stabilized Cu NCs, with wavelength-tunable emission, were stable in an aqueous medium under ambient conditions; they could easily be isolated and used for labeling cervical cancer HeLa cells. Cell viability studies indicated their noncytotoxic nature, making the NCs ideal for biological applications. The essential steps of the synthesis are depicted in Scheme 1.

Received: September 23, 2013
Accepted: February 26, 2014
Published: February 26, 2014

Scheme 1. Reaction Scheme for the Synthesis of Cu NCs in the Presence of Lysozyme[a]

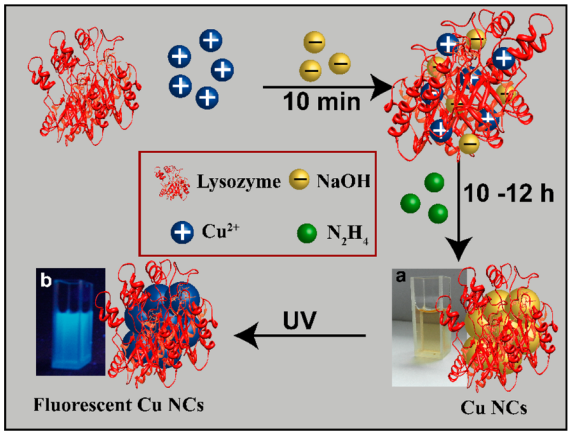

[a]Also included are the photographs of the products under (a) daylight and (b) UV light at 365 nm.

EXPERIMENTAL SECTION

Materials. Copper sulfate ($CuSO_4$), sodium hydroxide (NaOH), and hydrazine hydride (80%) were purchased from Merck Specialities Private Ltd., India. Lysozyme was purchased from Sisco Research Laboratories Pvt. Ltd. (SRL). 2,3-Bis(2-methoxy-4-nitro-5-sulfophenyl)-2*H*-tetrazolium 5-carboxanilide (XTT) and sinapinic acid for matrix-assisted laser desorption ionization (MALDI) analysis were purchased from Sigma-Aldrich USA. Milli-Q-grade water (18.2 MΩ·cm) was used for all of the experiments.

Synthesis of Cu NCs. $CuSO_4$ and lysozyme were mixed in water in a weight ratio of 2:1. The solution was stirred for 10 min at 45 °C, and then 0.04 mL of 1.0 M NaOH was added to adjust the pH to ∼10−11 when the color changed from blue to purple. To this was added 0.01 mM 80% N_2H_4, and the resulting solution was stirred for 6−12 h. The final color change of the solution was from purple to pale yellow. The same process for the synthesis was followed for different ratios of metal-to-protein concentration such as 2:1, 4:1, 6:1, and 8:1. For cell labeling and viability assay, Cu NCs were synthesized in a phosphate buffer at pH 7.4.

Characterization. Transmission electron microscopy (TEM) measurements were made using a JEOL JEM 2100 transmission electron microscope operating at a maximum accelerating voltage of 200 kV. The Cu NC dispersion was drop-cast onto carbon-coated Cu TEM grids and then kept for drying overnight at room temperature. UV−visible and fluorescence spectra were recorded with a Hitachi U-2900 or Perkin Elmer Lamda 25 and a Fluoromax-4 spectrophotometer instrument, respectively. Circular dichroism (CD) spectra were recorded using a Jasco J-815 machine. The instrument was calibrated with camphorsulfonic acid. All CD spectra were recorded at 25 °C, using a thermostatically controlled cell holder with a path length of 10 mm. ζ-potential measurements for samples were carried out using a Malvern zeta size Nano-ZS90 instrument at a temperature of 25 °C and a sample viscosity of 0.8872 mPa·s. Fourier transform infrared (FTIR) spectroscopic measurements were performed using a Perkin-Elmer Spectrum One spectrophotometer in the range 400−4000 cm^{-1}. X-ray diffraction (XRD) measurements were made using a Bruker AXS D8 Advance X-ray diffractometer fitted with a Cu $K\alpha_1$ source. Cellular labeling studies were carried out using a epifluorescence microscope (Nikon eclipse). For MALDI-time-of-flight (TOF) mass spectrometry (MS) analysis, an Applied Bio systems 4800 Plus MALDI TOF/TOF analyzer was used with sinapinic acid as the matrix. X-ray photoelectron spectroscopy (XPS) measurements for Cu NCs were performed by using a PHI 5000 VersaProbeII scanning XPS microprobe. Samples were prepared as pellets and introduced into the XPS prechamber under ultrahigh-vacuum conditions. Time-resolved fluorescence intensity decay of the NCs was recorded using a Life Spec II spectrofluorimeter. The sample was excited by a 375 nm laser light source. The decay curves were analyzed by *FAST* software, provided by Edinburgh Instruments along with the fluorimeter. The curves were fitted into the function

$$I(t) = \sum \alpha_i \exp(-t/\tau_i) \quad (1)$$

where α_i is the initial intensity of the decay component i, having a lifetime of τ_i.

The average lifetime of Cu NCs was calculated using the equation

$$\langle \tau \rangle = \frac{\sum_i \alpha_i \tau_i^2}{\sum_i \alpha_i \tau_i} \quad (2)$$

Quantum Yield Measurement of Cu NCs. Quantum yield measurement was carried out by dissolving quinine sulfate in 0.1 M H_2SO_4 (used as the reference) according to the standard protocol.[23] The Cu NC dispersion was used as such. The absorbance of the respective sample was measured on a Perkin-Elmer LS 55 UV−visible spectrophotometer. The quantum yield was calculated from the equation

$$Q = Q_R \frac{m_s}{m_r} \frac{n_s^2}{n_r^2} \quad (3)$$

where Q is the quantum yield of Cu NCs, Q_R is the quantum yield of quinine sulfate, m_s is the slope of the plot of integrated fluorescence intensity versus absorbance of Cu NCs, m_r is the slope of the plot of integrated fluorescence intensity verses absorbance of reference quinine sulfate, and n_s and n_r are the refractive indices of the sample and reference, respectively, in distilled water, which are assumed to be equal to that of water (1.33). The emission spectra for the samples were recorded at the excitation wavelength of 360 nm, keeping the slit width at 2 nm.

Sample Preparation for MALDI-TOF MS Measurement. For MALDI-TOF MS analysis, an Applied Bio systems 4800 Plus MALDI TOF/TOF analyzer was used with sinapinic acid as the matrix. Spectra were collected in the linear positive mode with mid-mass. The matrix was prepared by dissolving 10 mg of sinapinic acid in a 1:3 mixture of acetonitrile and 0.1% trifluoroacetic acid, and water was used to make up the volume to 1.0 mL (i.e., 0.2 mL of acetonitrile, 0.6 mL of 0.1% trifluoroacetic acid, and 0.2 mL of water). The samples were prepared at 1:1, 1:2, and 1:3 ratios with samples and a matrix. The cluster dispersion, without dilution, was mixed thoroughly with the matrix mixture, and from it, 0.8 μL of the resulting mixture was used for spotting.

Agarose Gel Electrophoresis. The electrophoretic stability of a lysozyme and Cu NC mixture was pursued by an agarose gel electrophoresis study. This was performed in 0.8% agarose at 5 v/cm and was visualized under a UV transilluminator (with excitation at 305 nm).

Cell Culture. HeLa cells (human cervical carcinoma) were acquired from the National Centre for Cell Sciences, Pune, India, and cultured in Dulbecco's modified Eagle's medium (DMEM) supplemented with 10% (v/v) fetal bovine serum obtained from PAA Laboratories, Austria, in a 5% CO_2 humidified incubator at 37 °C.

Cell Viability Assay. Cell viability assays were carried out as per the following. Cells (1×10^4 cells/well) were seeded in a 96-well microplate and grown in DMEM for 24 h in the presence of 5% CO_2 at 37 °C. Then various concentrations of Cu NCs (2.3−34.5 μg/mL) were added to the cells and kept for 24 h in similar conditions, which was followed by XTT assay as per standard manufacturer protocol. For the reaction, 7.0 μL of XTT was added to each well of the microplate and kept for 2 h for the formation of formazan. The control experiment was carried out in a similar way with various amounts of lysozyme. All of the experiments were carried out in triplicate. The percentage of cell viability of the control was taken as 100%. The cell viability was calculated based on the following formula:

$$\%\ \text{viable cells} = \frac{(A_{450} - A_{650})\ \text{of NC treated cells}}{(A_{450} - A_{650})\ \text{of control cells}} \times 100$$

dx.doi.org/10.1021/am500040t | *ACS Appl. Mater. Interfaces* 2014, 6, 3822−3828

The absorbances at 450 and 650 nm (A_{450} and A_{650}) correspond to the formation of formazan and the control medium, respectively.

Epifluorescence Microscopy. For cell imaging, 1×10^4 HeLa cells were seeded in a 35 mm cell culture plate and grown for 24 h. Cu NCs were added to the plate and incubated for another 2 h. Then, the medium was removed, and the cells were washed with phosphate-buffered saline (PBS) several times. Finally, 1 mL of PBS was added to the plate, and the cells were observed under an epifluorescence microscope (Nikon ECLIPSE TS100, Tokyo). An excitation band-pass filter for UV (340−380 nm) and an emission band-pass filter (435−485 nm) were used for cellular imaging.

Hemolysis Assay in Vitro. A total of 2.0 mL of human blood was centrifuged at 3000 rpm for 10 min to obtain human red blood cells (HRBCs). After removal of the supernatant, the HRBCs were washed with physiological buffer (PBS), which was followed by centrifugation. HRBCs so collected were suspended in deionized water. Portions of 0.1 mL of the HRBC suspension were added to 0.9 mL each of deionized water and PBS buffer, considered as positive and negative controls, respectively. Then experiments were performed in five different concentrations of a Cu NC composite. For each experiment, 0.1 mL of a stock HRBC suspension was added to 0.9 mL of a Cu NC composite with different concentrations (which varied from 0.6 to 4.5 μg/mL). All samples were incubated at 37 °C in a water bath for 3 h. After 3 h, the samples were centrifuged at 3000 rpm for 10 min, and the absorbance of the supernatants at 541 nm was recorded. The percentage of hemolysis of the Cu NC suspension was calculated by using the equation

$$\%\ \text{of hemolysis} = \frac{\text{O.D. of Cu NCs} - \text{O.D. of negative control}}{\text{O.D. of positive control} - \text{O.D. of negative control}} \times 100$$

where O.D. corresponds to the absorbance values of HRBCs at 541 nm. The hemolysis assay was performed in triplicate.

RESULTS AND DISCUSSION

Cu NCs were synthesized by treating a mixture containing a 2:1 molar ratio of $CuSO_4$ and lysozyme with N_2H_4 (0.01 mM) at pH 10−11 at 45 °C with constant stirring for 10−12 h. The medium, after reaction, appeared intense blue under a UV lamp, indicating the formation of Cu NCs (Scheme 1). The UV−visible spectrum (Figure 1A) of the reaction mixture recorded after 12 h did not exhibit the presence of any discernible peak. However, a gradual increase in extinction below 475 nm could be observed. An identical experiment in the absence of N_2H_4 did not result in such a bright-blue coloration, evidencing the role of N_2H_4 in the synthesis (Figure S1 in the Supporting Information, SI). Cu NCs, as evidenced from a strong fluorescence intensity, formed readily in the presence of hydrazine with high yield, as observed from fluorescence spectra (Figure S1 in the SI). They were reasonably stable in the presence of hydrazine after preparation at ambient conditions. In the absence of hydrazine, the fluorescence intensity decreased quickly with time (Figure S2 in the SI), thus indicating the additional role of hydrazine in stabilizing the NCs.

On the other hand, when the concentration ratio of $CuSO_4$/lysozyme was increased to 4:1 and beyond, a clear surface plasmon resonance (SPR) peak due to Cu NPs could be observed, occurring at 550 nm (Figure S3 in the SI). Thus, the studies reported in the present work were limited to products formed from a mixture of 2:1 molar ratio of $CuSO_4$ and the protein. The fluorescence spectrum of the product consisted of a single peak with a maximum at 450 nm, when excited by 360 nm light (Figure 1B). The excitation spectrum consisted of a single peak with a maximum at 360 nm (Figure 1B). The

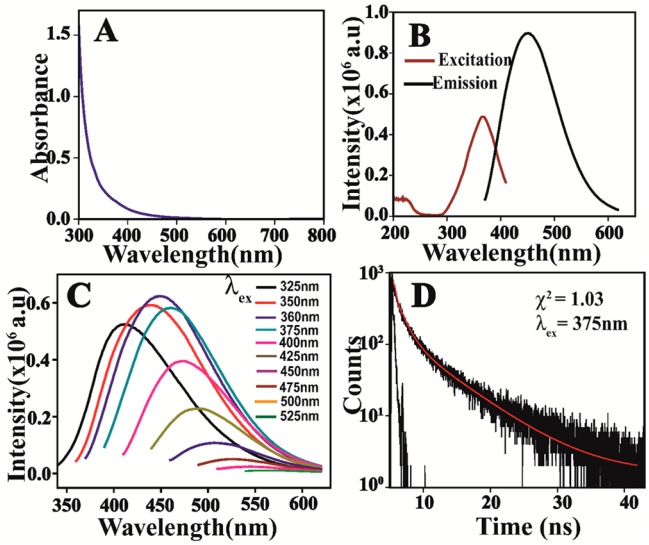

Figure 1. (A) Absorption spectrum of the product of the reaction of $CuSO_4$ and N_2H_4 in the presence of lysozyme. (B) Excitation and emission spectra of the product. (C) Excitation-dependent emission spectra of the product. (D) Fluorescence decay profile (λ_{ex} = 375 nm and λ_{em} = 450 nm) of the product.

fluorescence quantum yield was measured as 18% (λ_{ex} = 360 nm) with reference to quinine sulfate (54%) as the standard (Figure S4A in the SI).

Interestingly, the emission spectrum was found to be wavelength-tunable, with the emission maximum shifting from 410 to 575 nm, when the excitation wavelength was changed from 325 to 525 nm (Figures 1C and S4B in the SI). In the absence of N_2H_4, a similar product might have been formed; however, the fluorescence intensity of the product was less than that synthesized in the presence of N_2H_4 (Figure S5A in the SI). Also, the emission spectrum of the product formed in the absence of N_2H_4 did not exhibit clear wavelength-tunable properties like that formed in the presence of N_2H_4 (Figures S5A and S5B in the SI). The control experiment in the absence of $CuSO_4$ also indicated the presence of fluorescent species (Figure S6 in the SI); however, the intensity of fluorescence was either small or the peak occurred at shorter wavelength (Figure S6 in the SI). Also, the wavelength-tunable emission was not observed. Additionally, time-resolved fluorescence measurements indicated a clear difference between the products formed in the presence and absence of $CuSO_4$. For example, the average lifetime of emission of the product obtained from $CuSO_4$ and lysozyme was measured to be 6.5 ns (Figure 1D), whereas that in the absence of $CuSO_4$ was found to be 1.8 ns (Figure S7 and Table S2 in the SI). The emission characteristics of the product formed from the reaction match those reported for Cu NCs.[24] Thus, in the medium, Cu NCs were likely formed in the presence of the protein. Hydrazine acted as the reducing agent, producing Cu^0 from Cu^{2+} present in the medium. It was also observed that Cu NCs so produced (in the presence of hydrazine) were stable as the fluorescence emission did not change even after 15 days under ambient conditions (Figure S8 in the SI).

TEM measurements indicated the presence of small Cu NCs forming aggregates of average size of 2.3 ± 0.7 nm (Figure 2A,B). It is important to note here that the average particle size in Figure 2B appears to be higher than that of typical NCs. However, it is also known that when metallic NCs are

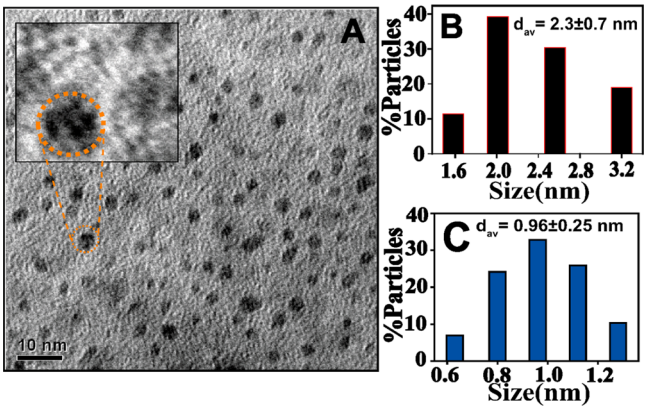

Figure 2. (A) TEM images of the product containing agglomerates of different sizes (scale bar 10 nm). The inset is the enlarged image of one of agglomerated particles. (B) Size histogram of different sizes of the particles (agglomerates). (C) Size histogram of individual clusters present inside the agglomerated product.

generated in the absence or presence of additional capping agents, agglomerated structures are formed, leading to an apparent higher particle size and even increased luminescence.[18,24,25] In the case of lysozyme, Au NCs formed agglomerated nanosized structures larger than individual NCs.[25,26] The average size of individual Cu NCs inside the aggregates (inset in Figure 2A and Figure 2C) was calculated as 0.96 ± 0.25 nm. Further probing of the sample using high-resolution TEM (HRTEM) showed the presence of crystalline particles with a lattice spacing of 0.207 nm, corresponding to the (111) plane of Cu^0.[27] The image is included in the SI (Figure S9). However, it may be stressed here that crystalline particles so observed might have been nonemissive and may represent larger SPR-active Cu nanoparticles. On the other hand, a crystalline lattice of ultrasmall atomic clusters of Cu may not be observed in HRTEM. Additionally, the population of larger crystalline Cu nanoparticles might have been rather small in the medium and thus not to have exhibited a clear SPR peak in the UV−visible spectrum.

The powder XRD pattern of the composite showed a broad peak at around 22° and the absence of characteristic peaks due to Cu (Figure S10 in the SI). The results also support a lack of crystallinity of the Cu NCs so formed and the absence of a significant population of crystalline Cu nanoparticles in the sample (consistent with a larger population of small-sized NCs).

FTIR spectra of lysozyme and lysozyme-stabilized Cu NCs are presented in Figure S11 in the SI. Three amide bands (amides I, II and III) due to the protein and occurring at 1600−1700, 1480−1575, and 1229−1301 cm^{-1}, respectively,[28,29] were present in the spectra. In addition, the peaks at 3400−3000 cm^{-1} due to −NH and −OH stretching vibrations were prominent in the spectra. The presence of functional groups such as $-NH_2$, −COOH, and −SH in the protein lysozyme may provide stability to the NCs. In a strongly alkaline medium, the protein might have been partially unfolded, thereby exposing a sufficient number of such groups that would facilitate attachment of the NCs to the protein.[30] It may also be true that the three-dimensional structure of the protein, with its functional groups separated spatially, provides enough room for attachment of more than one cluster to the same protein.

Among the three coinage metals, Cu is easily oxidized because of its low reduction potential. Therefore, it was deemed important to establish the oxidation state of Cu in the composite. For this, XPS analysis was performed for confirmation of the oxidation state of Cu in the Cu NC samples (Figure 3). Two prominent peaks, observed at 952.1

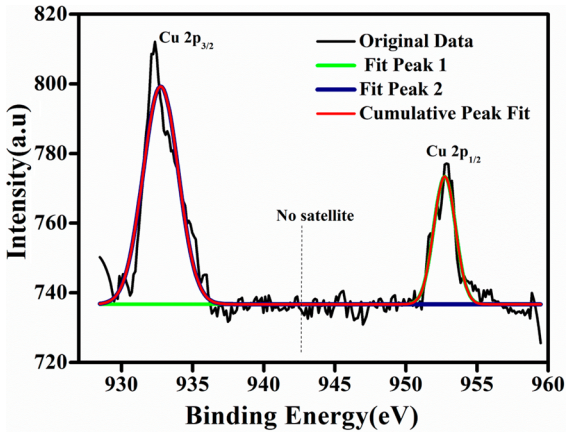

Figure 3. XPS spectrum of Cu 2p electrons in Cu NCs. The absence of satellite peaks indicated the absence of Cu^{2+}.

and 932.2 eV, were assigned to Cu $2p_{1/2}$ and Cu $2p_{3/2}$, which were characteristic peaks due to Cu^0. The absence of peak due to Cu^{2+} at 942 eV indicated that the Cu NCs did not contain Cu^{2+}. However, because the peak due to Cu^+ (932.3 eV) occurs at 0.1 eV apart from Cu^0, its presence cannot be ruled out. Further, the binding energy of sulfur (S) 2p observed at 162.8 eV (Figure S12 in the SI) indicated the presence of chemisorbed S on the surface of Cu NCs, which is supportive of the presence of Cu and S on the sample.[31,32]

Further analysis was carried out using MALDI-TOF MS to determine the core size of the Cu NCs. The spectrum was recorded in the linear positive mode, using a sinapinic acid matrix. The peak due to lysozyme appeared at 14300 Da (Figures 4 and S13 in the SI) because of its monocation form. It is expected that the molecular weight of a lysozyme/Cu NC composite will have peaks at masses higher than 14300 Da. A series of peaks in the region of 14300−14900 Da were observed. However, four peaks were prominent, which appeared at m/z 14300, 14434, 14564, and 14874 Da, as in

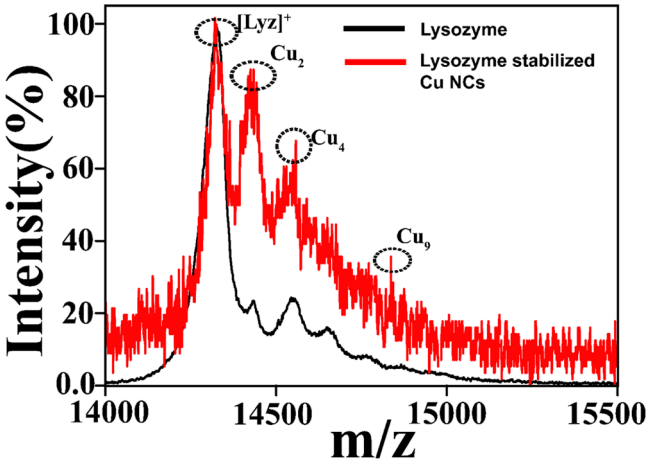

Figure 4. MALDI-TOF MS spectra of lysozyme (black line) and lysozyme-stabilized product (red line) with assignment of the characteristic peaks due to Cu NCs (dotted circles).

dx.doi.org/10.1021/am500040t | ACS Appl. Mater. Interfaces 2014, 6, 3822−3828

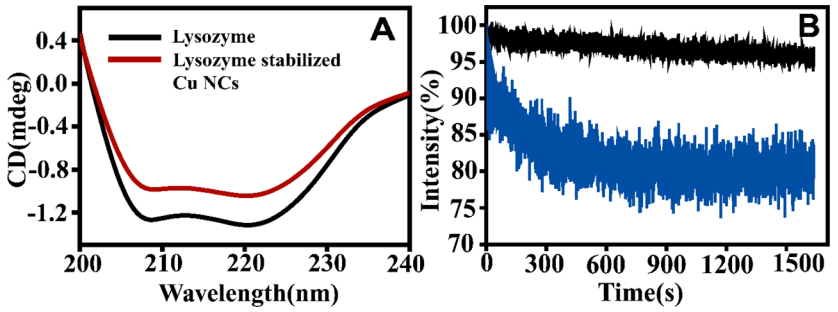

Figure 5. (A) CD spectra of lysozyme (black line) and as-synthesized Cu NCs (wine red) in the presence of lysozyme, exhibiting changes in the helicity of the α-helical structure following synthesis. (B) Representative time trace of fluorescence emission of Cu NCs (black line) showing slower decay in comparison to organic fluorophore, rhodamine 6G (blue line), under the same conditions.

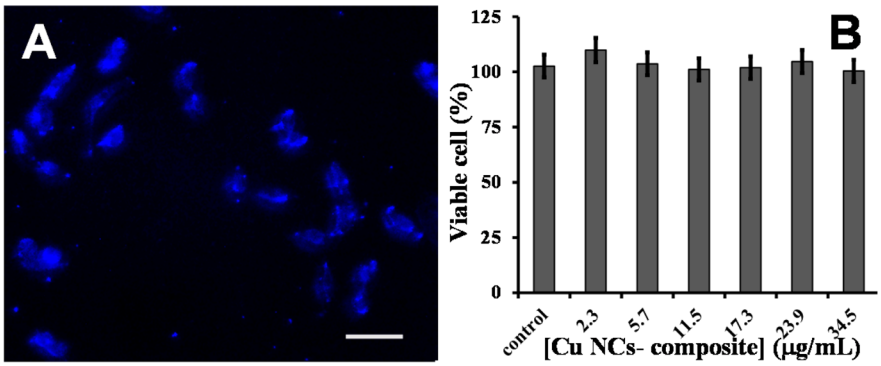

Figure 6. (A) Epifluorescence microscopic images of HeLa cells under UV light. Cells were incubated with Cu NCs for 2 h (scale bar 50 μm). (B) Cell viability for measuring the cytotoxicity of the Cu NCs on HeLa cells as measured by XTT assay after 24 h of incubation.

Figure 4. They can be attributed to $[Lyz]^+$, $[Lyz + Cu_2]^+$, $[Lyz + Cu_4]^+$, and $[Lyz + Cu_9]^+$, respectively. The results thus indicated the formation of Cu_2, Cu_4, and Cu_9 NCs, which were the same as those reported.[17,24,33] It is plausible that other clusters were also formed; however, they were not clearly detected in the MALDI-TOF MS spectrum.

CD measurements indicated a decrease in the α-helix content of the proteins present in the product medium from 52 to 45% following cluster formation (Figure 5A and Table S3 in the SI). Denaturation of the protein (even partially) consequent upon possible breakage of disulfide bonds,[26] or otherwise, might have led to agglomeration, accompanying the formation of Cu NCs at 45 °C. Additionally, the photostability of NCs is one of the properties that finds use in bioimaging and biolabeling applications. As shown in Figure 5B, fluorescence of the present Cu NCs remained nearly constant under continuous irradiation, with a fluorescence decrease rate of only 0.04%/min. In comparison, fluorescence of an organic fluorophore, rhodamine 6G, decreased at a rate of 0.23%/min with the photoirradiation time. The excellent resistance to photobleaching exhibited by the present Cu NCs, along with a considerable Stokes shift in the emission wavelength, makes a strong case for their use for cellular labeling and imaging. Additionally, an agarose gel electrophoresis study revealed the electrophoretic stability of NCs stabilized by the protein (Figure S14 in the SI).

In order to probe the surface charge of the synthesized Cu NCs, ζ-potential measurements were performed (Table S4 in the SI). The as-synthesized composite had a ζ-potential value of −28.1 mV, indicating an overall negative charge of the composite. Further, the potentials measured at the medium pH values of 9.0 and 4.5 were found to be −32.4 and −19.3 mV, respectively. The pH dependence of the ζ potential could be due to contribution from the protein, in addition to that of the clusters.

Further, it was deemed important to probe the effect of the pH on the fluorescence of the NCs. The NCs were synthesized at pH 11; the emission peak (at 450 nm) was found to be stable for 2 weeks. On the other hand, when the pH was made acidic, there was no change in the fluorescence, as was observed until an acidic pH of 4.3. The results are presented in the SI (Figure S15). The observation of pH-independent emission of Cu NCs indicates their importance for applications over a large pH range.

Cell Imaging and Cell Viability Test by XTT Analysis. An in vitro toxicity study of the NCs was examined by the XTT-based cell viability assay. XTT assay was performed to probe the cytotoxicity of the Cu NC composite by incubation in HeLa cells. The concentration of the composite used was 2.3−34.5 μg/mL. It should be mentioned here that the amount of Cu present in the composite, i.e., excluding lysozyme and hydrazine, was found to be 0.3−4.5 μg/mL. The Cu concentration is calculated based on the initial Cu salt taken for the reaction and assuming full conversion of the salt to Cu NCs. This means that the metal concentration reported here is the upper limit. The results indicated that Cu NCs had little or no cytotoxicity even at considerably higher concentration. HeLa cells (cervical cancer) in DMEM were incubated with different concentrations of Cu NCs in standard cell culture conditions. Following 24 h of incubation, the viability of the cells was determined, and the results are shown in Figure 6B. From XTT assay, it was found that more than 98% cells were viable upon incubation with 34.5 μg/mL of the Cu NC composite. The results indicated that the Cu NCs had no toxic

effect even at a considerably higher starting concentration of Cu.

The noncytotoxicity and high fluorescence quantum yield and photostability of the Cu NCs made it possible to test their suitability for cell labeling. This was pursued by incubating HeLa cells with Cu NCs for 2 h in DMEM. After removal of the medium, the cells were washed thoroughly with PBS (pH 7.4) to remove free unbound Cu NCs and finally were observed under a fluorescence microscope. The cells in the image (Figure 6A) could easily be observed under UV light (340−380 nm) because they appeared bright blue, which is the characteristic color of the Cu NCs. The corresponding image under a bright field and merged images are shown in Figure S16 in the SI. In comparison, control cells and cells treated with lysozyme did not exhibit any such fluorescence (Figures S17 and S18 in the SI). This clearly demonstrated the utility of the so-synthesized Cu NCs in live cell labeling.

Blood compatibility assay is an essential and initial requirement for the administration of any material in vivo such as hemolysis.[34] For that, preliminary investigations were performed using blood serum treated with Cu NCs. There was no loss of fluorescence (Figure S19 in the SI). On the other hand, there was an increase in fluorescence, which could be due to reducing the nature of the environment in the serum. The hemocompatibility of various concentrations of Cu NCs were performed by hemolysis assay. The results (Figures S20 and Figure S21 in the SI) demonstrated that Cu NCs did not cause significant hemolysis; i.e., they were hemocompatible at the concentrations used for the bioimaging and cell viability assay (0.6−4.5 μg/mL), which is comparable to previous studies.[35] Thus, blood compatibility assay supported the potential of the composites (and thus Cu NCs) for applications in vivo.

CONCLUSION

In conclusion, bright-blue fluorescent Cu NCs have been synthesized through a simple one-step reduction of $CuSO_4$ by N_2H_4, using lysozyme as the stabilizer. The NCs showed high photoluminescence quantum yield, excitation-tunable fluorescence, high photostability, and colloidal stability. They could be used for labeling HeLa cells. In conjunction with the photoluminescence properties, their low cytotoxicity would make them an ideal choice for biological and biomedical applications. The composite is comprised of Cu and lysozyme, where Cu is an essential trace element present in the body and lysozyme, an antimicrobial enzyme, is substantially present in a number of secretions, such as tears, saliva, etc. Thus, the composite might be considered to be biocompatible. The observed stability of the composite, coupled with the retention of fluorescence at physiological pH, is important for applications in vitro as well as in vivo.

ASSOCIATED CONTENT

Supporting Information

Additional fluorescence spectra, quantum yield calculations, MALDI-TOF MS analysis, XPS spectra, time-resolved fluorescence spectra, agarose gel electrophoresis analysis, bioimaging of cells with lysozyme, and blood compatibility studies in vitro. This material is available free of charge via the Internet at http://pubs.acs.org.

AUTHOR INFORMATION

Corresponding Authors

*E-mail: anumita@iitg.ernet.in.

*E-mail: arun@iitg.ernent.in.

Notes

The authors declare no competing financial interest.

ACKNOWLEDGMENTS

We acknowledge the Department of Science and Technology (DST Grant SR/S1/PC-30/2008), and Department of Biotechnology, Government of India, for financial support. We thank Subhamoy Banerjee and Upashi Goswami for help with the cell culture. We acknowledge help from the Department of Physics and Meteorology, IIT Kharagpur, with XPS analysis.

REFERENCES

(1) Wu, X.; He, X.; Wang, K.; Xie, C.; Zhou, B.; Qing, Z. Ultra Small Near-Infrared Gold Nanoclusters for Tumor Fluorescence Imaging in Vivo. *Nanoscale* **2010**, *2*, 2244−2249.

(2) Lin, C.-A. J.; Yang, T.-Y.; Lee, C.-H.; Huang, S. H.; Sperling, R. A.; Zanella, M.; Li, J. K.; Shen, J.-L.; Wang, H.-H.; Yeh, H.-I.; Parak, W. J.; Chang, W. H. Synthesis, Characterization, and Bioconjugation of Fluorescent Gold Nanoclusters Toward Biological Labeling Applications. *ACS Nano* **2009**, *3*, 395−401.

(3) Thompson, D.; Hermes, J. P.; Quinn, A. J.; Mayor, M. Scanning the Potential Energy Surface for Synthesis of Dendrimer-Wrapped Gold Clusters: Design Rules for True Single-Molecule Nanostructures. *ACS Nano* **2012**, *6*, 3007−3012.

(4) Sahoo, A. K.; Banerjee, S.; Ghosh, S. S.; Chattopadhyay, A. Simultaneous RGB Emitting Au Nanoclusters in Chitosan Nanoparticles for Anticancer Gene Theranostics. *ACS Appl. Mater. Interfaces* **2014**, *6*, 712−724.

(5) Shen, Z.; Duan, H.; Frey, H. Water-Soluble Fluorescent Ag Nanoclusters Obtained From Multiarm Star Poly(acrylic acid) as "Molecular Hydrogel" Templates. *Adv. Mater.* **2007**, *19*, 349−352.

(6) Petty, J. T.; Zheng, J.; Hud, N. V.; Dickson, R. M. DNA-Templated Ag Nanocluster Formation. *J. Am. Chem. Soc.* **2004**, *126*, 5207−5212.

(7) Richards, C. I.; Choi, S.; Hsiang, J.-C.; Antoku, Y.; Vosch, T.; Bongiorno, A.; Tzeng, Y.-L.; Dickson, R. M. Oligonucleotide-Stabilized Ag Nanocluster Fluorophores. *J. Am. Chem. Soc.* **2008**, *130*, 5038−5039.

(8) Xie, J.; Zheng, Y.; Ying, J. Y. Protein-Directed Synthesis of Highly Fluorescent Gold Nanoclusters. *J. Am. Chem. Soc.* **2009**, *131*, 888−889.

(9) Guével, X. L.; Hötzer, B.; Jung, G.; Hollemeyer, K.; Trouillet, V.; Schneider, M. Formation of Fluorescent Metal (Au, Ag) Nanoclusters Capped in Bovine Serum Albumin Followed by Fluorescence and Spectroscopy. *J. Phys. Chem. C* **2011**, *115*, 10955−10963.

(10) Mathew, A.; Sajanlal, P. R.; Pradeep, T. A Fifteen Atom Silver Cluster Confined in Bovine Serum Albumin. *J. Mater. Chem.* **2011**, *21*, 11205−11212.

(11) Chaudhari, K.; Xavier, P. L.; Pradeep, T. Understanding the Evolution of Luminescent Gold Quantum Clusters in Protein Templates. *ACS Nano* **2011**, *5*, 8816−882.

(12) Lin, Y.-H.; Tseng, W.-L. Ultrasensitive Sensing of Hg^{2+} and CH_3Hg^+ Based on the Fluorescence Quenching of Lysozyme Type VI-Stabilized Gold Nanoclusters. *Anal. Chem.* **2010**, *82*, 9194−9200.

(13) Zhou, T.; Haunq, Y.; Li, W.; Cai, Z.; Luo, F.; Yanq, J. C.; Chen, X. Facile Synthesis of Red-Emitting Lysozyme-Stabilized Ag Nanoclusters. *Nanoscale* **2012**, *4*, 5312−5315.

(14) Liu, C.-L.; Wu, H.-T.; Hsiao, Y.-H.; Lai, C.-W.; Shih, C.-W.; Peng, Y.-K.; Tang, K.-C.; Chang, H.-W.; Chien, Y.-C.; Hsiao, J.-K.; Cheng, J.-T.; Chou, P.-T. Insulin-Directed Synthesis of Fluorescent Gold Nanoclusters: Preservation of Insulin Bioactivity and Versatility in Cell Imaging. *Angew. Chem., Int. Ed.* **2011**, *50*, 7056−7060.

(15) Wen, F.; Dong, Y.; Feng, L.; Wang, S.; Zhang, S.; Zhang, X. Horseradish Peroxidase Functionalized Fluorescent Gold Nanoclusters for Hydrogen Peroxide Sensing. *Anal. Chem.* **2011**, *83*, 1193−1196.

(16) Kawasaki, H.; Hamaguchi, K.; Osaka, I.; Arakawa, R. pH-Dependent Synthesis of Pepsin-Mediated Gold Nanoclusters with Blue Green and Red Fluorescent Emission. *Adv. Funct. Mater.* **2011**, *21*, 3508−3515.
(17) Kawasaki, H.; Kosaka, Y.; Myoujin, Y.; Narushima, T.; Yonezawa, T.; Arakawa, R. Microwave-Assisted Polyol Synthesis of Copper Nanocrystals without Using Additional Protective Agents. *Chem. Commun.* **2011**, *47*, 7740−7742.
(18) Vilar-Vidal, N.; Blanco, M. C.; López-Quintela, M. A.; Rivas, J.; Serra, C. Electrochemical Synthesis of Very Stable Photoluminescent Copper Clusters. *J. Phys. Chem. C* **2010**, *114*, 15924−15930.
(19) Jia, X.; Li, J.; Han, L.; Ren, J.; Yang, X.; Wang, E. DNA-Hosted Copper Nanoclusters for Fluorescent Identification of Single Nucleotide Polymorphisms. *ACS Nano* **2012**, *6*, 3311−3317.
(20) Tapiero, H.; Townsend, D. M.; Tew, K. D. Trace Elements in Human Physiology and Pathology. Copper. *Biomed. Pharmacother.* **2003**, *57*, 386−398.
(21) Gaggelli, E.; Kozlowski, H.; Valensin, D.; Valensin, G. Copper Homeostasis and Neurodegenerative Disorders (Alzheimer's, Prion, and Parkinson's Diseases and Amyotrophic Lateral Sclerosis). *Chem. Rev.* **2006**, *106*, 1995−2044.
(22) Cater, M. A.; Fontaine, S. L.; Shield, K.; Deal, Y.; Mercer, J. F. ATP7B Mediates Vesicular Sequestration of Copper: Insight Into Biliary Copper Excretion. *Gastroenterology* **2006**, *130*, 493−506.
(23) Lakowicz, J. R. *Principles of Fluorescence Spectroscopy*, 2nd ed.; Kluwer Academic/Plenum Publishers: New York, 1999.
(24) Jia, Z.; Li, J.; Wang, E. Cu Nanoclusters with Aggregation Induced Emission Enhancement. *Small* **2013**, *9*, 3873−3879.
(25) Xu, H.; Suslick, K.S. Water-Soluble Fluorescent Silver Nanoclusters. *Adv. Mater.* **2010**, *22*, 1078−1082.
(26) Baksi, A.; Xavier, P. L.; Chaudhari, K.; Goswami, N.; Pal, S. K.; Pradeep, T. Protein-Encapsulated Gold Cluster Aggregates: The Case of Lysozyme. *Nanoscale* **2013**, *5*, 2009−2016.
(27) Qing, Z.; He, X.; He, D.; Wang, K.; Xu, F.; Qing, T.; Yang, X. Poly(thymine)-Templated Selective Formation of Fluorescent Copper Nanoparticles. *Angew. Chem., Int. Ed.* **2013**, *52*, 9719−9722.
(28) Shang, L.; Wang, Y.; Jiang, J.; Dong, S. pH-Dependent Protein Conformational Changes in Albumin: Gold Nanoparticle Bioconjugates: A Spectroscopic Study. *Langmuir* **2007**, *23*, 2714−2721.
(29) Surewicz, W. K.; Mantsch, J. H.; Chapman, D. Determination of Protein Secondary Structure by Fourier Transform Infrared Spectroscopy: A Critical Assessment. *Biochemistry* **1993**, *32*, 389−394.
(30) Chen, T.-H.; Tseng, W.-L. (Lysozyme Type VI)-Stabilized Au_8 Clusters: Synthesis Mechanism and Application for Sensing of Glutathione in a Single Drop of Blood. *Small* **2012**, *8*, 1912−1919.
(31) Wei, W.; Lu, Y.; Chen, W.; Chen, S. One-Pot Synthesis, Photoluminescence, and Electrocatalytic Properties of Subnanometer-Sized Copper Clusters. *J. Am. Chem. Soc.* **2011**, *133*, 2060−2063.
(32) Bensebaa, F.; Ellis, T. H.; Kruus, E.; Voicu, R.; Zhou, Y. Characterization of Self-Assembled Bilayers: Silver−Alkanethiolates. *Langmuir* **1998**, *14*, 6579−6587.
(33) Jia, X.; Yang, X.; Li, J.; Li, D.; Wang, E. Stable Cu Nanoclusters: From an Aggregation-Induced Emission Mechanism to Biosensing and Catalytic Applications. *Chem. Commun.* **2014**, *50*, 237−239.
(34) Wu, H. X.; Zhang, S. J.; Zhang, J. M.; Liu, G.; Shi, J. L.; Zhang, L. X.; Cui, X. Z.; Ruan, M. L.; He, Q. J.; Bu, W. B. A Hollow-Core, Magnetic, and Mesoporous Double-Shell Nanostructure: In Situ Decomposition/Reduction Synthesis, Bioimaging, and Drug-Delivery Properties. *Adv. Funct. Mater.* **2011**, *21*, 1850−1862.
(35) Chandra, V. S.; Baskar, G.; Suganthi, R. V.; Elayaraja, K.; Joshy, M. I.; Beaula, W. S.; Mythili, R.; Venkatraman, G.; Kalkura, S. N. Blood Compatibility of Iron-Doped Nanosize Hydroxyapatite and Its Drug Release. *ACS Appl. Mater. Interfaces* **2012**, *4*, 1200−1210.